www.DeepakPublishing.com

Rawashdeh, S., et al. (2013): JoSS, Vol. 2, No. 1, pp. 85-104
(Peer-reviewed Article available at www.jossonline.com)

www.JoSSonline.com

Aerodynamic Stability for CubeSats at ISS Orbit

Samir A. Rawashdeh and James E. Lumpp, Jr.

Space Systems Laboratory, Electrical and Computer Engineering, University of Kentucky, Lexington, KY

Abstract

At altitudes below 500 km, satellites experience a significant amount of aerodynamic drag that can be utilized to stabilize satellites to align with the relative wind direction. Designing a non-rotating spacecraft such that the center of pressure is behind the center of mass provides an aerodynamic restoring torque, which in combination with an oscillation damping system provides stability and alignment with the spacecraft velocity vector. Passive aerodynamic stability and damping has been demonstrated on orbit by the Soviet Union on Cosmos-149 and Cosmos-320 in 1967 and 1970, respectively, and by NASA on the Passive Aerodynamically Stabilized Magnetically-damped Satellite (PAMS) spacecraft, deployed from STS-77 in 1996. This paper presents our analysis of aerodynamic stability solutions for the CubeSat domain. CubeSat form factors are significantly smaller and lighter than the previous flight demonstrations; moreover, they must fit inside a CubeSat launcher, and only deploy aerodynamic elements post orbit-insertion. We describe completely passive solutions for 3U and 1U CubeSats, where aerodynamic fins are deployed and magnetic hysteresis material is used for oscillation damping. We also show that greater velocity vector alignment can be achieved using active rate damping, using a magnetometer and magnetic torque coils running the B-dot control law to provide improved oscillation damping. Component selections are offered to create off-the-shelf aerodynamically stable CubeSat platforms, and we conclude that passive aerodynamic stability is suitable for the altitude and inclination of upcoming CubeSat flight opportunities on International Space Station (ISS) crew re-supply missions.

1. Introduction

Passive attitude stabilization, in general, is an attractive attitude control solution for satellites when coarse pointing is required, especially if power, mass, and volume are constrained. Tuning and designing the spacecraft to specific geometric, mass, and magnetic properties can provide passive attitude control, without the need for active sensors or actuators.

Magnetic, gravity gradient, and aerodynamic torques are the main sources of moments on Small Satellites in Low Earth Orbit (LEO). Solar radiation pres-

sure is also an important factor for satellites with significantly large surface areas. A satellite can be designed to amplify one of these forces to overcome the others to achieve stability. For example, several CubeSats employed passive magnetic stabilization, where permanent magnets align the satellite with Earth's magnetic field, to provide antenna or sensor pointing (Rawashdeh and Lumpp, 2010; Cutler et al., 2010). CubeSats have also been designed to deploy gravity booms to create a gravity gradient bias and achieve nadir pointing (Waydo et al., 2002). In addition, aerodynamic torquing in low orbits can be used to achieve velocity-vector pointing, which is the focus of this paper.

Angular rate damping must accompany these stabilization techniques (Rawashdeh, 2009). While the environmental torques would provide restoring torques necessary for stability, a form of angular rate damping is necessary to reach a steady-state condition. The use of active attitude control actuators, such as reaction wheels or magnetic torque coils, can help to achieve angular rate damping, at the cost of their added complexity. There are also simple passive solutions that require no power and processing capabilities (and have fewer failure modes) such as the inclusion of magnetic hysteresis material (Rawashdeh, 2009; Levesque, 2003), particle dampers, and fluid dampers (Abel, 2011).

The Soviet Union and NASA have successfully demonstrated passive aerodynamic stability on orbit on larger than CubeSat-class satellites. In addition, aerodynamic stability with active damping has been demonstrated on a 3U CubeSat. The research described in this paper focused on the feasibility of completely passive solutions for 1U and 3U CubeSat designs that can be built with commercial off-the-shelf components. Active damping using magnetic torque coils is also considered, for improved steady-state performance.

Aerodynamic stability has been shown to be feasible for altitudes below 500 km. In conjunction with a passive damping solution, it provides a simple and low cost pointing solution. Velocity vector alignment is convenient for spacecraft dipole antenna pointing or when a sensor requires its aperture to track the velocity vector, for example, for atmospheric plasma measurements or Earth horizon sensing. The design of the CubeSats in this work feature deployable drag fins (resembling a shuttlecock) that provide their attitude aerodynamic stability. The increased drag area caused by the fins reduces its orbital lifetime to be on the order of months for ISS altitudes, which is desirable in many cases to mitigate orbital debris concerns.

SpaceX reports that a significant number of CubeSat launch opportunities are expected to become available on upcoming crew re-supply missions to the International Space Station (ISS), , each mission carrying up to four CubeSat deployers (Bjelde, 2011). From an attitude control point of view, satellites at this relatively low altitude are dominated by aerodynamic torques as shown in Table 1. This will drive complexity and limit the feasibility of common attitude control schemes that are not designed to counter disturbance torques of that magnitude. The designs presented in this paper utilize the strong aerodynamics for stability, and are proposed to be simple and low cost alternatives that are suitable for short-term and reoccurring experimental missions on ISS crew re-supply launches.

Table 1. Environmental Torques in General Regions of Influence (adapted to metric units from Schrello, 1961).

Regions of Influence	Altitude Range	Environmental Effects
Region I	Below 300 km	Aerodynamic torques dominate angular motion
Region II	300-650 km	Aerodynamic and Gravitational torques are comparable
Region III	650-1000 km	Aerodynamic, Gravitational and Solar torques are comparable
Region IV	Above 1000 km	Solar and Gravitational torques dominate angular motions

This paper discusses aerodynamic stability solutions for the CubeSat domain and suggests alternatives that are capable of providing passive stabilization for

ISS altitude and inclination. The attitude propagator described herein is used to observe the satellite's dynamic response and steady-state behavior caused by aerodynamic torques, while also taking into account perturbing torques due to gravity gradient and magnetic effects. Stability characteristics and pointing errors are shown for three spacecraft designs based on off-the-shelf components.

2. Background

At altitudes near the Kármán line (100 km), the Knudsen number typically begins to exceed 1, indicating that the atmosphere more accurately corresponds to a rarefied, free-molecular flow regime than a continuum flow regime (Wertz, 1978). Therefore, an approach based on free-molecular aerodynamics or direct simulation of individual atmospheric particles on the satellite is necessary. Atmospheric drag for small satellites becomes a prominent source of disturbance and angular moments in the low part of LEO, at altitudes of 500 km and below. Atmospheric density decreases exponentially as a function of altitude, and atmospheric drag effects become minimal at higher altitudes. Table 1 summarizes the relative magnitudes of aerodynamic, gravity gradient and solar torques as a function of altitude. Note that the region boundaries in Table 1 are inexact, and are affected by the spacecraft design. For example, satellites with large cross-sectional areas will experience significant solar radiation torques at lower altitudes, and a symmetric satellite does not experience significant gravity gradient torques.

The earliest research on satellite rotational dynamics caused by the residual atmosphere, and the concept of utilizing these forces for stability, dates back to the late 1950s and early 1960s (Schrello, 1961; Wall, 1959). The selected references here include mathematical models and a number of proposed aerodynamically stable designs, and conclude that aerodynamic stability can be achieved at altitudes around 300 miles (483 km) and below, that several concepts show theoretical feasibility, and that oscillatory behavior is expected, necessitating angular rate damping for stability.

The Soviet Union conducted the first on-orbit demonstrations of aerodynamically stabilized satellites, in 1967 (Cosmos 149) and in 1970 (Cosmos 320) (Wade, 2012; Sarychev et al., 2007; Sarychev et al., 1984; Sarychev and Ovchinnikov, 1994). The two spacecraft were known as "space arrows" because of their extended aerodynamic skirt stabilizers. Figure 1 is a photograph of a museum model of the space arrow. Damping was achieved with the use of two gyroscopes connected to the satellite body through viscous-spring restraints that dissipate energy when satellite oscillations cause gyroscope precession. The satellite weighed 375 kg, was in orbit at 48.4° inclination, and operated in altitudes between 246 and 326 km.

Figure 1. Cosmos 149 (K.E. Tsiolkovsky State Museum of The History of Cosmonautics, 2004-2012).

Aerostabilization in LEO was also flight tested as an experiment on the shuttle Endeavour in 1996 (NASA JSC, 1996). The Passive Aerodynamically Stabilized Magnetically-damped Satellite (PAMS) experiment demonstrated the feasibility of aerostabilization with magnetic hysteresis material for damping. The PAMS

satellite had a cylindrical "stove pipe" design, with a significantly thicker shell on one end to shift the center of mass of the satellite and produce an aerodynamically stable design for altitudes from 250 to 325 km (Kumar, et al., 1996; Kumar et al., 1995; Pacini and Skillman, 1995).

The NASA simulations for PAMS were based on free-molecular aerodynamics and incorporated variations in atmospheric density, global winds, and solar radiation. They also simulated the behavior of hysteresis material cycling in a model of the Earth's magnetic field, and showed damping within 1 day, and a worst-case cone angle of 9°. The actual flight experiment was deemed a success after several rendezvous operations (NASA GSFC, 1996). Figure 2 shows PAMS with the shuttle Endeavour in view.

Figure 2. NASA photo of PAMS taken from Shuttle Endeavour (NASA GSFC, 1996).

3. Previous Work on CubeSats

The dimensions of PAMS are similar to those of CubeSats (see verification section); however, the CubeSat standard does not allow such an offset in the center of mass unless a shift is performed post-deployment. In the design studied here, a "shuttlecock" design is used as an effective way to shift the center of drag pressure behind the center of mass after orbit insertion while still conforming to the CubeSat standard that requires that the center of mass lies within 2 cm of the geometric center (CalPoly, 2012).

Psiaki proposed a shuttlecock design to obtain aerodynamic stability on a 1U CubeSat (Psiaki, 2004). The system uses four deployable "feathers" that resemble retractable tape measures extending from a 1U CubeSat body. It also incorporates active magnetic torque coils for damping, and was shown through simulation to achieve stability for all altitudes below 500 km. The design was evaluated by comparing a simplified stiffness model with a model based on free-molecular aerodynamics. The narrow one-meter-long feathers were deployed at 12°. The design was shown to stop tumbling within one hour, and achieved a steady-state pointing error of 2° within 15 hours.

In previous work at the University of Kentucky Space Systems Laboratory, the authors investigated the conditions of stability of a 3U CubeSat with deployable side panels. We completed a one-degree-of-freedom analysis on the effect of varying panel lengths and deployment angles for the 3U form factor at varying altitudes in the presence of gravity gradient moments (Rawashdeh et al., 2009). In other research, a six- degree-of-freedom orbit and attitude propagator was developed with models for aerodynamic, gravity gradient, permanent magnet, and magnetic hysteresis material torques (Rawashdeh, 2009). The attitude propagator was mainly used to support KySat-1, a 1U CubeSat manifested on NASA's ElaNa-1 mission, in designing satellites with permanent magnet attitude stability systems with hysteresis material for angular rate damping. The propagator, called Smart Nanosatellite Attitude Propagator (SNAP), was verified by simulating several spacecraft of known designs, including PAMS, and comparing the simulations with their on-orbit results (Rawashdeh and Lumpp, 2010). In our study, we improved on the aerodynamic modeling by increasing the fidelity of the geometric representation, as well as improving the magnetic hysteresis model to be a continuous and smooth mathematical model, and introducing a model for active magnetic control. Then we leverage the SNAP simulation tool and previous studies on general stability across altitudes and propose aerodynamically stable CubeSat designs for the ISS altitude using commercially available components, and use the propagator to simulate the satellites' attitude response in all degrees of freedom.

The most recent development described in public literature in aero stabilized CubeSats is by the U.S. Naval Research Laboratory, where two 3U CubeSats employed aerodynamic fins to provide correcting torques for velocity-vector pointing (Armstrong et al., 2009). A suite of active attitude control actuators (reaction wheels and torque coils) was used to augment the passive aerodynamic torques and provide angular rate damping. These QbX spacecraft were modeled after the Pumpkin Inc. Colony-I CubeSat Bus, where four deployables change the geometry to achieve an aerodynamic bias, as shown in Figure 3. The QbX "space darts" were launched in 2010, successfully demonstrating the feasibility of aerodynamic stabilization for a 1U CubeSat at an altitude of 300 km (U.S. NRL, 2010; Arnold et al., 2012).

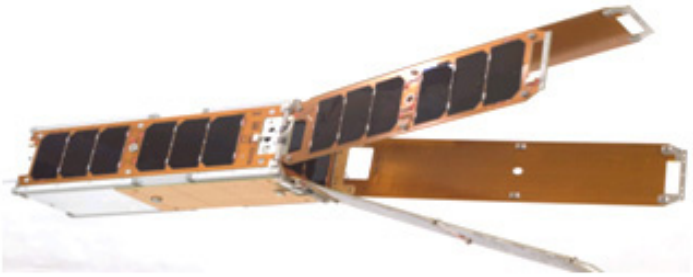

Figure 3. Pumpkin Colony-1 Bus. Photo courtesy of (Pumpkin Inc., 2012).

The QbX satellites showed the feasibility of aerodynamic control, but damping was achieved through a complex system involving a suite of active actuators. There have been no published flight demonstrations of completely passive solutions for CubeSats. In this paper, we use magnetic hysteresis material for angular rate damping. The Pumpkin Inc. Colony-I Bus is also studied, as well as a 1U CubeSat with 25 cm fins made of 1-inch wide tape measure.

4. Simulator

The Smart Nanosatellite Attitude Propagator (SNAP) is a 6-DOF satellite attitude propagator implemented in MATLAB® and Simulink® that can be used to analyze the environmental torques affecting a satellite and to design and analyze passive attitude stabilization techniques, such as passive magnetic stabilization, gravity gradient stabilization, and aerodynamic stabilization. The propagator includes: a simple two-body gravitational model for orbit propagation, in addition to models for gravity gradient torque, magnetic torque due to permanent magnets, magnetic hysteresis torque and damping, aerodynamic torques, and Magnetic B-dot control. SNAP, with a subset of features, has been made publicly available by the University of Kentucky Space Systems Laboratory (University of Kentucky, 2013). This section describes portions of the attitude propagator implemented in Simulink® that include the attitude dynamics components relevant to the scope of this paper and new for this research.

Figure 4 (next page) shows the high-level view of the Simulink® implementation of SNAP with the relevant force and moment models for this work. The satellite's 6-DOF states and body dynamics are implemented in the center block, which has translational forces and rotational moments as inputs. The translational force is found using a two-body gravitational model to simulate orbital motion. Rotational moments are a sum of the environmental effects, namely gravity gradient, aerodynamics, and magnetic effects (either magnetic hysteresis material or active magnetic B-dot control, depending on the method of damping). Figure 4 illustrates the feedback elements for the orbital position, velocity, and attitude. The value of the forces and moments at each time step is a function of the satellite's position in orbit and its attitude at the previous time step. Simulink®'s solvers propagate the satellite's state with time, given the description of the dynamics.

The total external torque is found as the combination of the gravity gradient, aerodynamic, magnetic coil, and magnetic hysteresis moments, expressed as:

$$\mathbf{M_{total}} = \mathbf{M_{gg}} + \mathbf{M_{aero}} + \mathbf{M_{coils}} + \mathbf{M_{hysteresis}}$$

These models calculate the torque components caused by the respective environmental effects at a certain point in orbit as a function of the satellite mass and magnetic properties, the attitude at that point, the position in orbit, and the velocity in orbit. The individual torques are discussed in detail next.

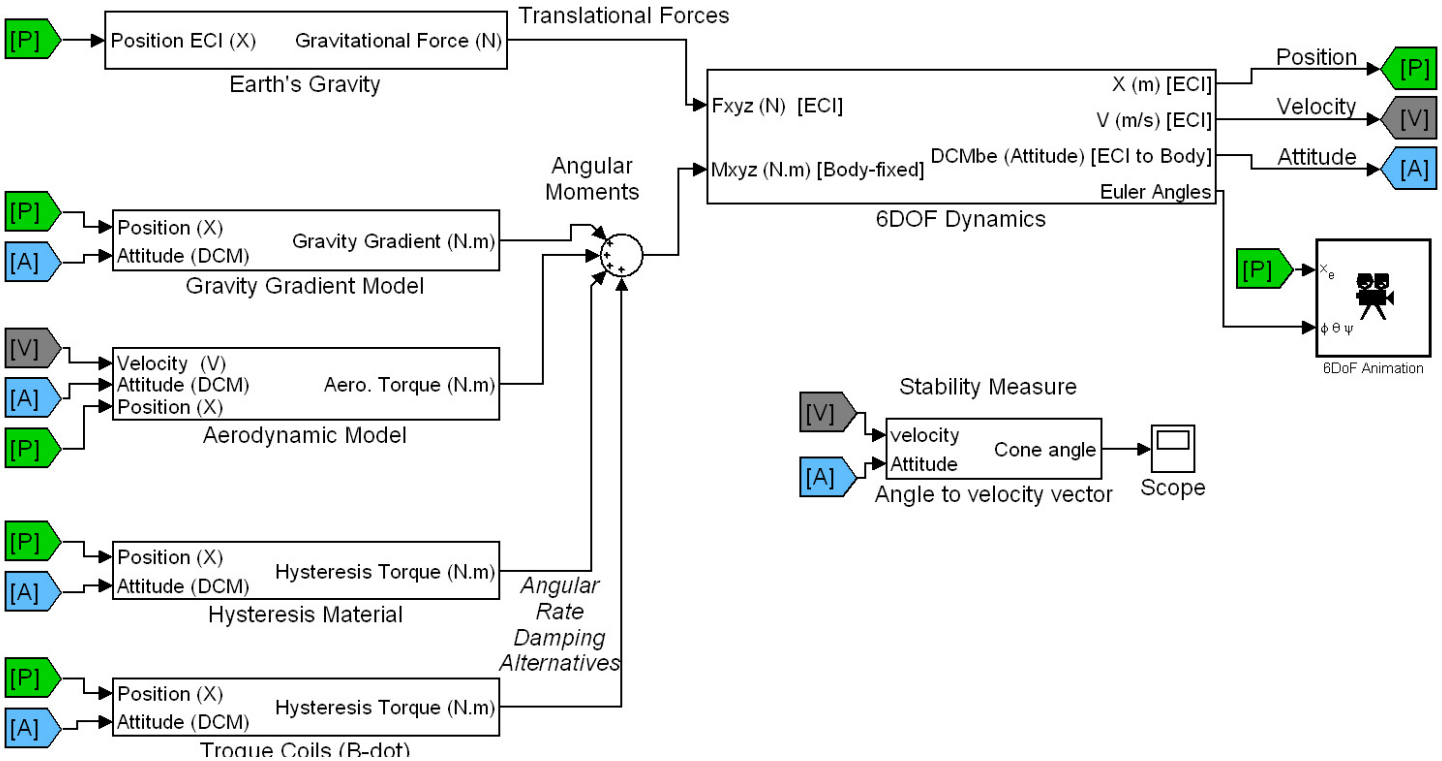

Figure 4. Simulink® Model of SNAP, the Smart Nanosatellite Attitude Propagator, with the models relevant to this work. The Hysteresis Material and Torque Coils models are alternatives for passive and active damping (only one is used).

4.1 Gravity Gradient Torque

As shown in Table 1, gravity gradient torque is a prominent source of disturbance moments for aerodynamically stabilized satellites for orbits below 500 km. This is also evident in the literature where other sources of disturbances are considered minute and are ignored (Schrello, 1961; Wall, 1959; Sarychev and Ovchinnikov, 1994; Kumar et al., 1995). The gravity gradient torque for an Earth-orbiting satellite is caused by differences in the distance to Earth across the satellite body; mass that is closer to Earth experiences higher gravitational attraction. An asymmetric body in a gravitational field will experience a torque tending to align the axis of least inertia with the field direction (Sidi, 1997).

The mass distribution of the satellite is adequately described in the inertia matrix. The torque caused by the gravity gradient effect is modeled in the Attitude Propagator as:

$$\mathbf{M_{gg}} = \frac{3\mu}{R_0^{\,3}}\,\mathbf{u_e} \times \mathbf{J}\mathbf{u_e} \quad \text{(N)},$$

where $\mathbf{M_{gg}}$ is the gravity gradient torque, $\mathbf{u_e}$ is the unit vector towards nadir, R_0 is the distance from the center of Earth to the satellite, $\mathbf{J}$ is the inertia matrix μ, is the geocentric gravitational constant (Larson & Wertz, 1999; Wie, 1998).

This equation is modeled in Simulink® to calculate the gravity gradient torque at each time step, given the position in orbit which defines the distance R_0, and the current attitude, which is used to find the nadir vector u_e expressed in body-frame coordinates.

4.2 Aerodynamic Torque

The amount of aerodynamic torque a satellite experiences is a function of atmospheric density, the orientation relative to the wind vector (velocity vector), the aggregate forward-facing area (accounting for shadowing), the coefficient of drag, and the moment arm that the center of pressure acts upon with respect to the center of mass. In rarefied atmospheric conditions, the aerodynamic torque for a certain area element can be

calculated by:

$$\mathbf{M}_{\mathbf{aero}} = \frac{1}{2}\rho V^2 C_d A \left(\mathbf{u}_{\mathbf{v}} \times \mathbf{s}_{\mathbf{cp}}\right) \text{ (N)},$$

where $\mathbf{M}_{\mathbf{aero}}$ is the aerodynamic torque, uv is the unit velocity vector, $\mathbf{s}_{\mathbf{cp}}$ is the vector from the center of pressure to the center of mass, ρ is the atmospheric density, V is the satellite velocity, C_d is the drag coefficient (set to equal 2 in this work), and A is the affected area (Wertz, 1978; Larson & Wertz, 1999).

The aerodynamic torque for a certain attitude is a function of the area facing the velocity vector that is not shadowed by any other parts of the spacecraft body. Taking the torque that is due to aerodynamics into account requires a method of representing the spacecraft geometry. Then, an algorithm is needed to calculate the torque the spacecraft experiences given the geometric representation and the attitude of the satellite relative to the wind vector (negative velocity vector).

The geometry of the satellite is discretized into volumetric elements, as shown in Figure 9 in the analysis section, at a dot per 0.125 cm^3. A look-up table is generated that maps the attitude relative to the velocity vector to a torque factor that is later scaled by the atmospheric density and orbital velocity to find the aerodynamic torque the satellite experiences at that orientation. This torque profile is generated before the simulation runtime to reduce the number of computations and minimize the simulation duration. At runtime, the satellite's angle to the velocity vector (the incoming wind) is computed from the current attitude and orbit model. The look-up table returns the torque factor associated with that deflection angle. The mapping table is generated across a full range of satellite rotations, by considering elements directly facing the wind vector that are not shadowed by other satellite components. A form of numerical integration is performed by summing up the torque contributions of all the satellite elements to find the total torque affecting the satellite at a given attitude. Although shadowing is often ignored in literature when the main body of the satellite is small relative to the dimensions of the fins, this assumption cannot be made for the designs that will follow, where shadowing is an important factor to consider for CubeSat solutions. This geometric representation is a very convenient tool for solving this type of problem.

The look-up table is used at runtime to obtain a torque factor, described by $\frac{1}{2}C_d A\left(\mathbf{u}_{\mathbf{v}} \times \mathbf{s}_{\mathbf{cp}}\right)$, given the current satellite attitude. That value is then scaled by the atmospheric density (ρ) at that altitude using another look-up table, and the square of the satellite's orbital velocity (V^2) computed from the orbit propagator to find the final torque affecting the satellite at that time step.

4.3 Magnetic Torque Coils

Next, we develop the model for magnetic torque coils, which are used here as an alternative to provide angular rate damping for improved tracking accuracy. A magnetic dipole in a magnetic field experiences an angular moment that aligns the dipole with the magnetic field lines, like a compass needle pointing north. The torque affecting a satellite due to a magnetic dipole interacting with the Earth's magnetic field is modeled as:

$$\mathbf{M}_{\mathbf{coils}} = \mathbf{m} \times \mathbf{B}_{\mathbf{Earth}} \text{ (N)},$$

where $\mathbf{M}_{\mathbf{coils}}$ is the magnetic torque vector in body-frame, **m** is the magnetic dipole moment vector in Am^2 in body-frame, $\mathbf{B}_{\mathbf{Earth}}$ is the Earth magnetic flux density vector in body-frame (Sidi, 1997).

In this paper, the magnetic dipole moment **m** is generated using magnetic torque coils based on the popular B-dot control law:

$$\mathbf{m} = -K\,\dot{\mathbf{B}}_{\mathbf{Earth}} = -K\,\frac{d}{dt}\mathbf{B}_{\mathbf{Earth}} \text{ } (Am^2),$$

where **m** is the magnetic dipole moment vector, K is a tunable gain factor, and **B** is the Earth magnetic flux density vector in body frame (Silani & Lovera, 2002). The B-dot control law actuates the torque coils to counter any changes in the observed magnetic field. From the satellite perspective, variations in the magnetic

field caused by the satellite travel through orbit and the Earth's rotation are slower than the observed magnetic field variations caused by the satellites angular motion; therefore, the change in the observed magnetic field approximates the satellite angular rates. In effect, the B-dot control law acts to resist angular motion, and is an effective detumbling and damping solution.

The Earth's magnetic field is modeled as a dipole (L-Shell Model) (Wertz, 1978). Given the position in orbit at a given simulation step, the local magnetic field from the Earth can be found using the dipole model, and rotated to body-frame coordinates, given the attitude of the satellite. At runtime, given the Earth's magnetic field, and the satellite's orientation, the magnetic torque due to the magnetic dipole is found.

The active magnetic damping solution requires a set of magnetic torque coils, typically three that are installed orthogonally. It also requires knowledge of the magnetic field, which can be measured using a magnetometer. In this paper, active damping is only presented as a proof of concept and perfect knowledge of the magnetic field is assumed. An upper limit for the magnetic dipole per coil of 0.04 Am^2 is set, as a conservative number that can be achieved with air-core coils embedded in solar boards as traces across multiple layers. Solar boards with embedded torque coils and magnetometers are commercially available (GOM Space, 2012).

4.4 Magnetic Hysteresis Damping

While magnetic hysteresis material is a completely passive solution for angular rate damping, it is non-trivial to study and predict, and motivated the implementation of a simulation environment. Magnetically "soft" material of low coercivity can be magnetized by the Earth's magnetic field and follows hysteresis patterns as it cycles in a magnetic field. This makes it suitable as a means for angular rate damping for small-satellites in orbits with a significant magnetic field. Magnetic hysteresis is a physical property of ferromagnetic material. The material becomes magnetized when an external magnetic field is applied, forcing the magnetic domains on the atomic level to polarize. Depending on the magnetic remanence (*Br*) of the material, it will retain a magnetic dipole of some strength when the external magnetic field is removed. The magnetic coercivity (*Hc*) of the material is the intensity of the external magnetic field required to diminish the magnetization from saturation to zero when applied against the polarity of the material. The lag (or "hysteresis") in tracking the externally applied magnetic field caused by the coercivity and remanence of the material results in energy lost as heat in the material. The phenomenon can be thought of as the magnetic dipoles having "friction" when their orientation is forced to change.

Figure 5 shows a sample magnetization curve generated using the mathematical model of the hysteresis material used in this study (Flatley & Henretty, 1995). The mathematical recipe was developed to simulate the NASA PAMS satellite, and is a set of first order differential relationships that we implemented and introduced to the propagator for this work. The model is an improvement on previous parallelogram approximations (Rawashdeh, 2009) as the continuous non-switching nature of the curve adds fidelity to the simulations.

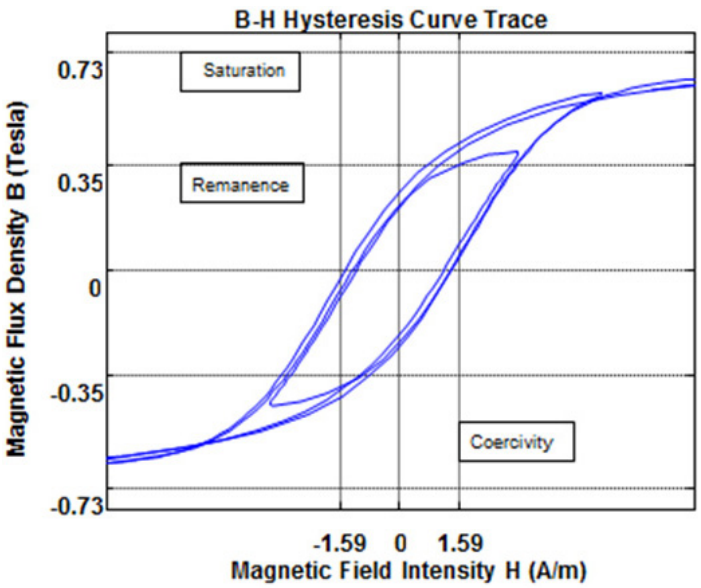

Figure 5. Trace of the hysteresis loop model of HyMu80.

Quantifying the amount of hysteresis material to include in a satellite design is challenging. The amount of damping caused by hysteresis material is not a fixed or calculated amount; it is a result of the behavior of the hysteresis material interacting and cycling through the

Earth's magnetic field. Modeling and simulation are a convenient and effective way to study hysteresis material (Levesque, 2003).

Several inexpensive alternatives are available commercially, most commonly as electric shielding material. For example, HyMu80, Carpenter 49, Permalloy 80, and Mumetal are high-permeability alloys that are suitable as magnetic hysteresis material for spacecraft rotation damping. HyMu80, which is selected for the proposed designs in this paper, has a coercivity of 1.59 Am^{-1}, remanence of 0.35 Tesla, and saturation of 0.73 Tesla.

5. NASA PAMS - Simulator Verification

As mentioned in the background section of this paper, the Passive Aerodynamically Stabilized Magnetically-damped Satellite (PAMS) demonstrated aerodynamic stabilization with magnetic hysteresis material for damping as an experiment on the shuttle Endeavour in 1996. Here, we use PAMS as a case study to verify the accuracy of the simulation environment that has been developed. Based on available information in publications and in NASA web archives on orbit injection and satellite design, Table 2 summarizes the simulation parameters. Figure 6 shows the representation of the satellite in SNAP and the computed torque profile, which shows the amount of torque PAMS experiences as a function of its deflection from the velocity vector. A characteristic of an aerodynamic stable configuration is a steep negative sloped zero-crossing, where positive error angles produce negative torques, and vice versa, causing the satellite to oscillate around the zero-crossing.

5.1 On-orbit observations

PAMS was launched in 1996 and observed to have a 0.5°/second initial tumble (NASA GSFC, 1996). The shuttle Endeavor performed several rendezvous operations to observe its attitude. PAMS was declared to have achieved velocity vector tracking stability under 20°, and to be a successful experiment in the STS-77 mission report (NASA JSC, 1996).

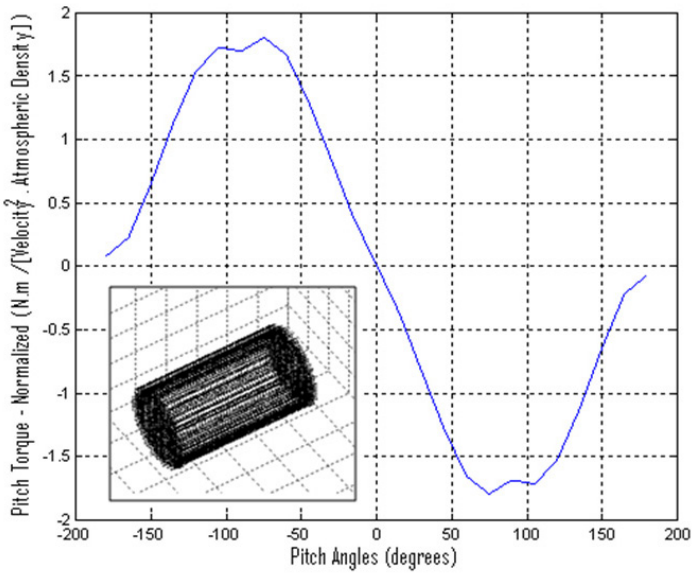

Figure 6. PAMS geometric representation and resulting torque profile. The torque profile shows the amount of correcting torque the satellite experiences vs. the error angle.

Table 2: Simulated PAMS design parameters, based on data in (Kumar et al., 1995; Kumar et al., 1996).

Orbit	283.4 km, 39° inclination
Mass	~12.4 kg, Center of mass 15 cm from leading end.
Dimensions	Cylindrical: 45cm long, 23.8 cm radius
Hysteresis	Three rods 1/75the volume of rods on TRANSIT 1B satellite
Inertia (Ixx, Iyy, Izz)	(0.11, 0.0815, 0.0815) kg m^2

5.2 Simulations Results

Figure 7 (next page) depicts the simulation response for the PAMS parameters in SNAP, described herein. The response shows the satellite settling to a cone angle just below 20° after 18 orbits, with some variability across different simulations, depending on the initial attitude and around which axis the initial tumble is applied. The simulations show similar damping effect and velocity vector tracking, given that configuration. The steady-state oscillatory behavior with a cone angle smaller than 20° matches the simulations

and observations performed by NASA (NASA GSFC, 1996).

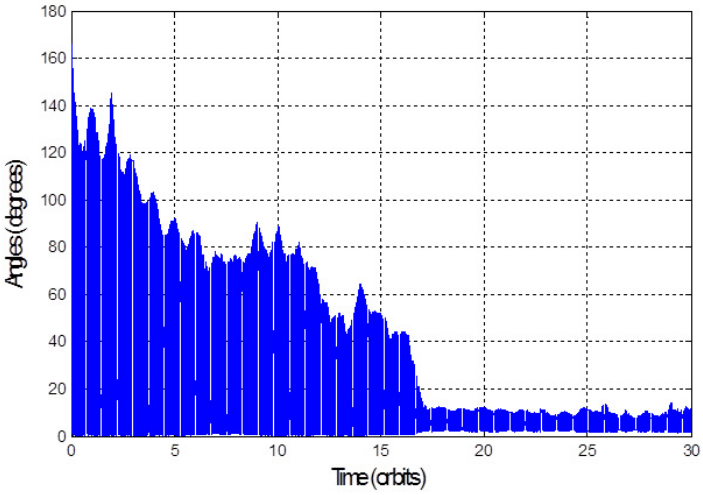

Figure 7. PAMS simulated attitude response. The plot shows the cone angle relative to the velocity vector.

6. Aerostabilized CubeSat Design

As discussed earlier, aerodynamic stability has been demonstrated with passive damping on the Cosmos Space Arrows and NASA PAMS, and proposed and demonstrated on CubeSats with active damping. An attitude propagator was developed, to study the feasibility of completely passive solutions while conforming to the CubeSat form factor.

Aerostabilized CubeSats are required to conform to the CubeSat mass limit (1.33 kg per 1U CubeSat) and the center of mass restriction, where the center of mass is required to be within two centimeters from the geometric center before deployment (CalPoly, 2012). This excludes the PAMS and Cosmos solutions, where the satellite is designed with a center of mass shift to create the aerodynamic bias, and any CubeSat solution would require that the separation between the center of pressure and center of mass be achieved after orbit insertion. The objective of the attitude solutions presented in this paper is to recover from the initial tumble after launch and then achieve and maintain velocity vector alignment in steady-state condition.

The designs presented are CubeSats with deployable side panels that are deployed to an acute angle measured from the negative velocity vector, as depicted in Figure 8. Before deployment, the panels lie against the sides of the satellite and the center of mass is near the geometric center. Deployment shifts the center of mass slightly, but shifts the center of drag pressure back further, providing correcting torques that can be used for velocity vector alignment.

In our previous research (Rawashdeh et al., 2009), the panel deployment angle, the length of the deployable side panels, and the orbit altitude were varied and simulated to analyze the effect of these variables on the steady-state behavior of the satellite. Figure 8 shows a set of torque profiles for three designs with a panel length of 20 cm deployed at angles of 10°, 30°, and 50° with respect to the vehicle centerline at an altitude of 400 km. The plots describe the amount of torque the satellite experiences as a function of its attitude to the velocity vector. The shape of the plot and the dips that occur in these profiles are a function of the satellite geometries, where significant shading may occur at certain attitudes. Negative sloped zero-crossings indicate stable points at which the satellite will settle temporarily or permanently; a positive error angle produces negative torque to realign the satellite to the stable point, and vice-versa.

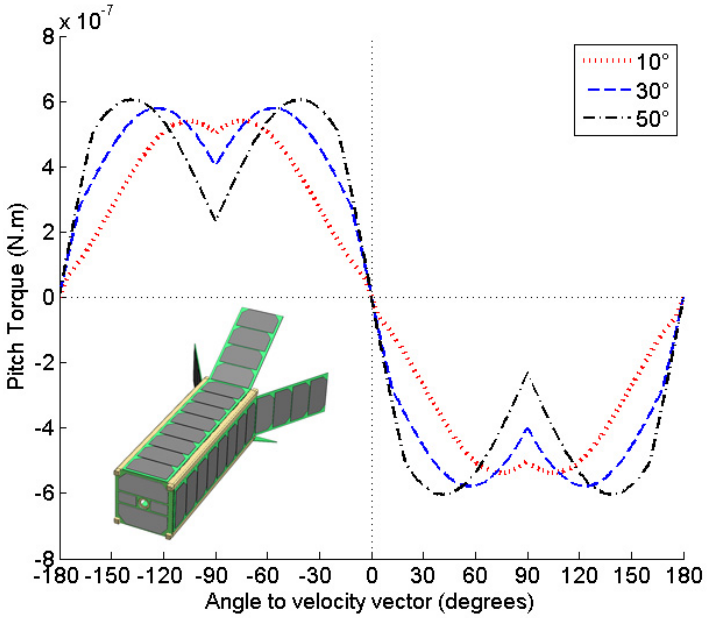

Figure 8. Torque Profiles at 400 km for 3U CubeSat with 20 cm long panels. The plots show the torque experienced as a function of the attitude angle to velocity vector. Roll angle is 0°.

An exhaustive search through the panel deployment angle, panel length, and orbit altitude was performed, to determine the optimal deployment angle and panel length. In general the panel length was found to mainly scale the torque profile in amplitude for panel lengths greater than 10 cm. Likewise, evaluating the torque profiles at lower altitudes with higher atmospheric density increases the torque experienced, and is manifested as a scaling in the torque profile. The main performance parameter considered was the amount of stiffness through the ram-facing angle. Stiffness is defined as the amount of correcting torque the satellite experiences for every 1° of error, which is calculated as the negative of the derivative of the pitch torque profile evaluated at the zero degree angle. Greater stiffness promises smaller steady-state errors and higher oscillation frequencies.

The torque profiles in Figure 8 provide considerable insight into how a geometric design would perform. It is evident that a deployment angle of 50° is most stiff through the zero crossing. It was found that angles beyond 50° begin to provide diminishing return in terms of stiffness. Another important factor to consider in the design is the amount of forward-facing area that directly affects the orbit lifetime.

7. 3U CubeSat with Deployable Side Panels

The first proposed design is based on the Pumpkin Inc. Colony-1 Bus (shown in Figure 3). Using the attitude propagator described earlier, several design configurations were tested and simulated. We present two geometries with two rate-damping solutions based on the Colony-1 Bus. For the first case study, the panels of the 3U CubeSat are designed to be deployed at 50°, which was found to be most stiff (i.e., it has the largest correcting torque for every degree of error).

Figure 9 describes the satellite dimensions and location of the center of mass, and shows the point cloud representation of this geometry. The torque profiles were generated across all roll angles; Figure 10 shows a cross section of the torque profile for this configuration.

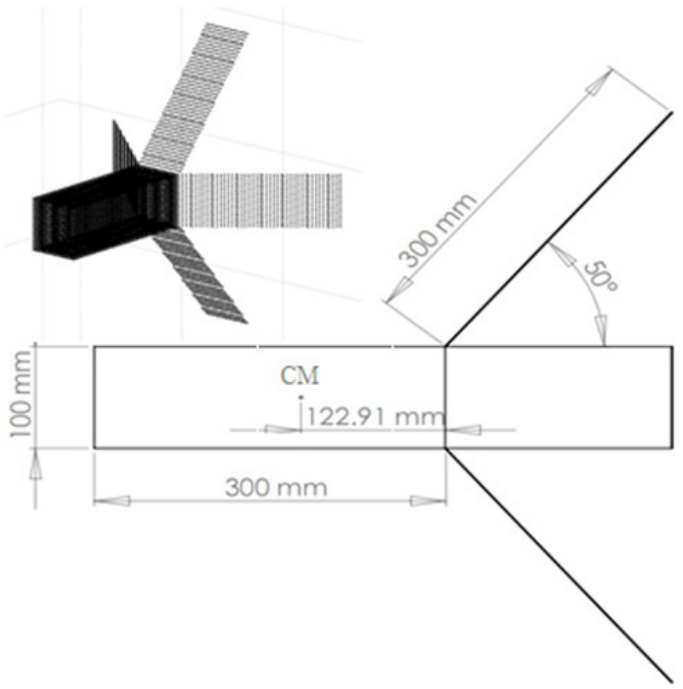

Figure 9. Design diagram of the 3U CubeSat, panels deployed at 50°, and the discretized representation for torque calculation.

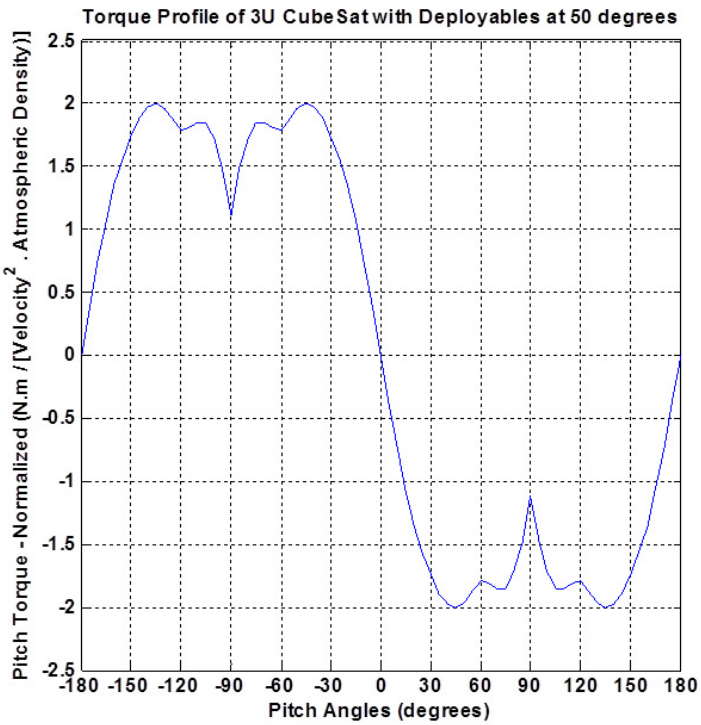

Figure 10. Torque profile at 45° roll angle, normalized to atmospheric density and velocity2, of 3U CubeSat with deployables at 50°.

Table 3 summarizes the design parameters and simulation results. For the passive solution, several simulations were conducted while parametrically varying the amount of hysteresis material, allowing the optimal amount of hysteresis material to be chosen. Given an initial tumble rate of 10°/second, the simulation shows that hysteresis losses successfully detumble the satellite and a steady-state condition is achieved below 20° between the forward-leading face and the velocity vector. The attitude response for the passive solution is shown in Figure 11. The steady-state behavior is an artifact of several counteracting torques. The aerodynamic torques work to correct for pointing errors, counteracting gravity gradient disturbance torques (significant for 3U solutions) and hysteresis material torques.

Table 3. Design parameters and simulation results for 3U CubeSat with panels deployed at 50°.

3U CubeSat, 10 cm x 30 cm fins deployed at 50°		
Design Type	Passive Damping Solution	Active Damping Solution
Orbit	380 km circular, 51.6° inclination	
Mass, Inertia (Ixx, Iyy, Izz) Drag Area	5 kg, (0.019, 0.06, 0.06) kg m^2 0.032981 m^2	
Angular Rate Damping	Hysteresis: HyMu80 10.5 cm^3 (3.5 cm^3 per axis)	B-dot control 0.04 Am^2 three-axis Torque Coils, K = 18000
Simulation Parameters	10 °/second initial rate	
Results		
Detumbling Time	5 hours	15 hours
Steady-state Tracking Accuracy	10-20°	Below 0.1°

Figure 12 shows the attitude response of the active solution that utilizes magnetic torque coils driven by the B-dot control law. Using the relatively low generated dipole moment, a tracking accuracy of 0.1° is achieved. The B-dot control gain was chosen to be K = 18000, resulting in an average total magnetic dipole of 0.000675 Am^2, with a maximum dipole of 0.002 Am^2 for any of the three coils in steady state. The plot demonstrates the feasibility of the B-dot damping approach in providing oscillation damping for velocity vector tracking. Magnetometer measurement noise and other non-idealities are expected to decrease the tracking precision.

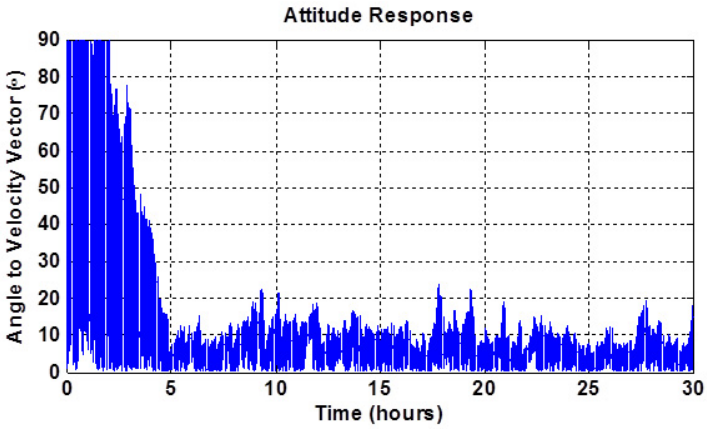

Figure 11. Simulated time response of aerostabilized 3U CubeSat with 30 cm panels deployed at 50° degrees and HyMu80 hysteresis damping.

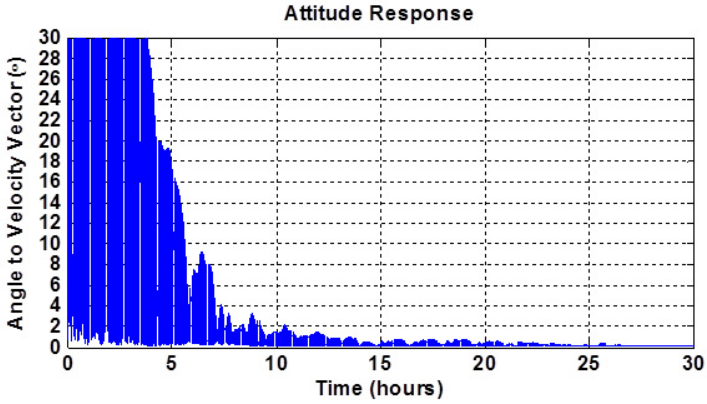

Figure 12. Simulated time response of aerostabilized 3U CubeSat with 30cm panels deployed at 50° degrees and magnetic B-dot damping.

8. 3U CubeSat with Lower Drag

A deployment angle of 50° was found to be most stiff, promising the greatest pointing accuracy. As Figures 11 and 12 show, coarse pointing can be achieved using hysteresis material, and fine pointing can be achieved using active magnetic damping. We note that a deployment angle of 50° results in a forward facing area of 0.033 m^2, as noted in Table 3.

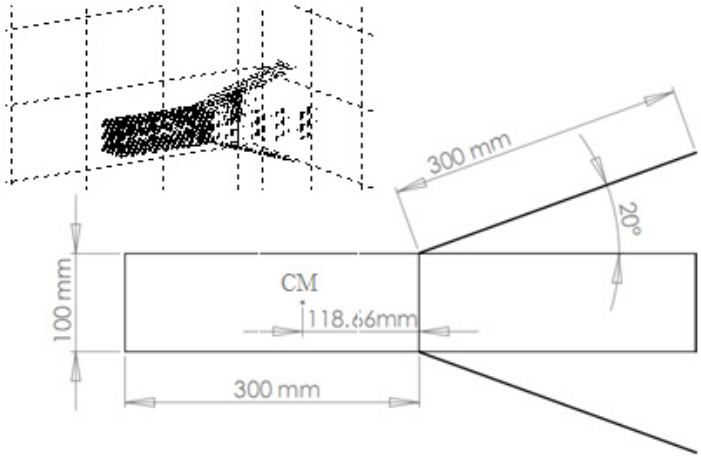

Figure 13. Design diagram of the 3U CubeSat, panels deployed at 20°, and the discretized representation used for torque calculation.

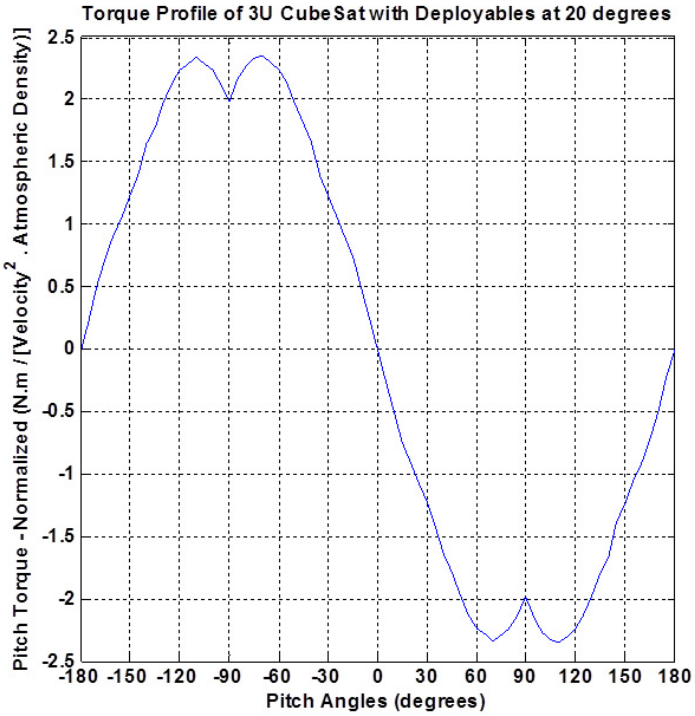

Figure 14. Torque profile at 45° roll angle, normalized to atmospheric density and velocity2, of 3U CubeSat with deployables at 20°.

The orbit lifetime associated with this drag area at ISS altitudes is on the order of 6 to 24 months, as found by the NASA Debris Assessment Software (DAS 2.0) as worst-case and best-case scenarios, depending on solar activity (NASA Orbital Debris Program Office). This lifetime may be considered desirable for short duration missions and for debris mitigation reasons.

The second 3U design, using a deployment angle of 20° (shown in Figure 13), is presented next. This configuration results in a forward-facing area of 0.02 m^2, and an expected orbit lifetime of 9 to 33 months. This configuration may also be desirable for solar power generation when incident light is expected to illuminate the side of the satellite and the drag fins are populated with solar cells to reduce the light incidence angle.

Figure 14 shows the torque profile for this configuration. We note that there is a small loss in stiffness where the magnitude of the slope through the zero-pitch attitude angle is less than it is for the 50° configuration. However, this does not have a great effect on the attitude response for the passive solution. Hysteresis material offers coarse pointing; there is no significant difference in the attitude response in Figure 15, compared to the previously presented solution and the attitude response in Figure 11.

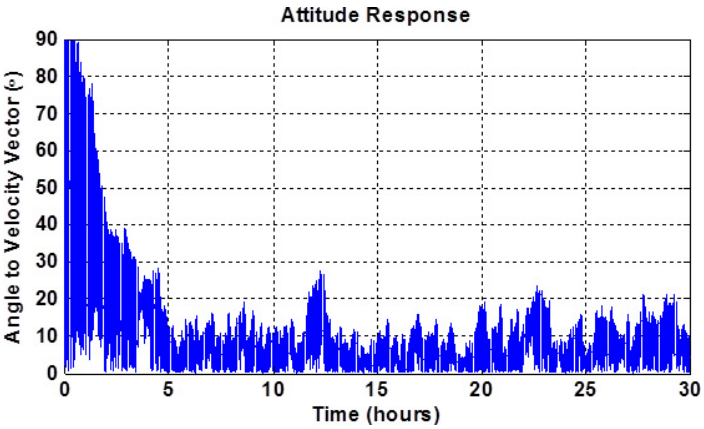

Figure 15. Simulated time response of aerostabilized 3U CubeSat with 30cm panels deployed at 20° and HyMu80 hysteresis damping.

The attitude response of the active damping alternative using magnetic torque coils driven by the B-dot control law is presented in Figure 16 (next page). Velocity vector tracking below 0.1° is achieved. The B-dot control parameters were identical to the previous 50°

deployment angle design. Table 4 summarizes the simulation parameters and results for the 3U solution with side panels deployed at 20°.

Table 4. Design parameters and simulation results for 3U CubeSat with panels deployed at 20°.

3U CubeSat, 10 cm x 30 cm fins deployed at 20°		
Design Type	Passive Damping Solution	Active Damping Solution
Orbit	380 km circular, 51.6° inclination	
Mass, Inertia (Ixx, Iyy, Izz) Drag Area	5 kg, (0.0109, 0.0664, 0.0664) kg m^2 0.020261 m^2	
Angular Rate Damping	Hysteresis: HyMu80 10.5 cm^3 (3.5 cm^3 per axis)	B-dot control 0.04 Am^2 three-axis Torque Coils, K = 18000
Simulation Parameters	10 °/second initial rate	
Results		
Detumbling Time	5 hours	20 hours
Steady-state Tracking Accuracy	15-20°	Below 0.1°

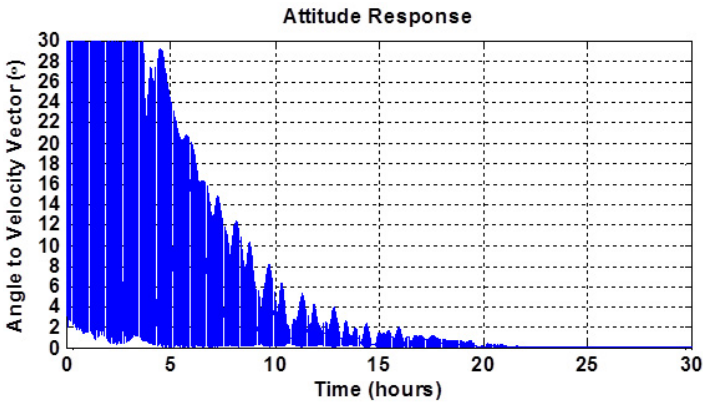

Figure 16. Simulated time response of aerostabilized 3U CubeSat with 30cm panels deployed at 20° and magnetic B-dot damping.

9. 1U CubeSat with Tape-Measure Fins

Next, we investigated the feasibility for a 1U CubeSat solution. The 1U CubeSat is the most frequent form factor and usually has the lowest launch cost. We present an aerodynamically stable design that is feasibly under the weight and volume limitations of the 1U form factor. The main design requirements were simplicity and manufacturability, especially since at this time no off-the-shelf frame can be bought to readily achieve aerodynamic stability on a 1U CubeSat. Dimensions and deployment of the drag fins were considered, as well as the volume required for hysteresis material and the placement of the magnetic coils, in the case of the active damping solution.

Figure 17 shows the 1U CubeSat design that employs drag fins that measure four 25 cm long and 2.5 cm wide. The fins, which can be constructed with using 1-inch wide flexible tape measure spring steel, can be wrapped around the satellite and tied down before deployment, similar to the antenna deployment mechanism on KySat-1 (Chandler, et al., 2007). Once released, the fins unravel and snap to their final intended positions.

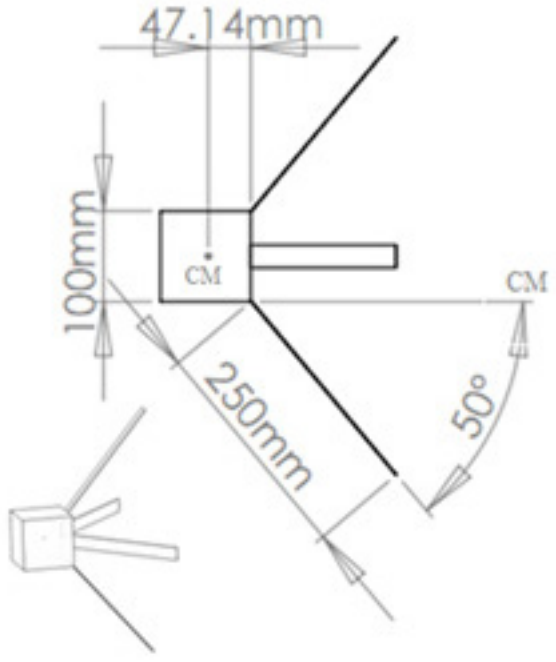

Figure 17. Design diagram of the 1U CubeSat design, 1" tape measure fins deployed at 50°.

A short enough fin length was selected so that the fins would not wrap around completely and interfere with other fins when stowed (under 30 cm length). A deployment angle of 50° was chosen to maximize restoration torque, and several simulations were run to find the most effective volume of hysteresis material. Figure 18 shows the torque profile for this design. This configuration has a significantly smaller magnitude of restoration torque compared to the 3U solutions presented earlier.

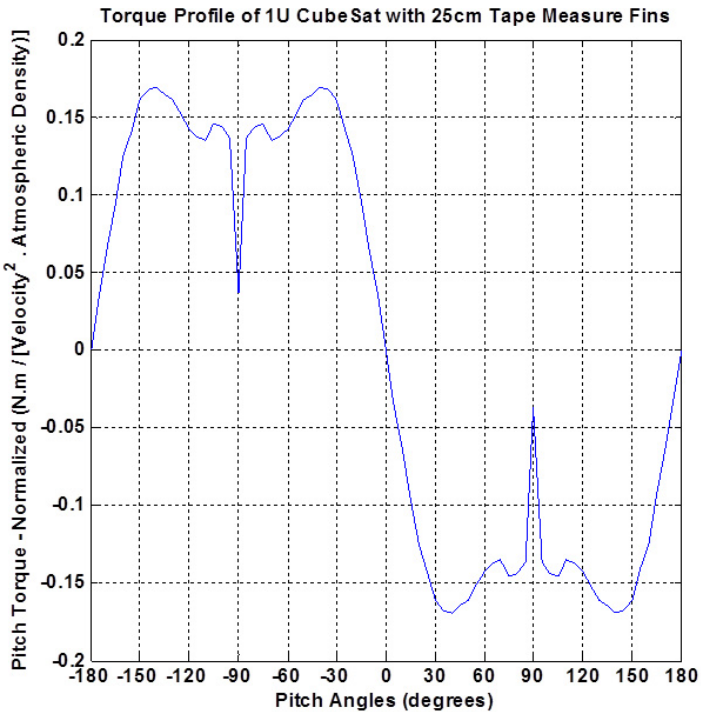

Figure 18. Torque profile at 45° roll angle, normalized to atmospheric density and velocity2, of 1U CubeSat with deployable fins at 50°.

However, gravity gradient torques, which are a function of the mass distribution of the satellite, are minimal for this design. The 1U form factor, being more symmetric, has an advantage over the 3U shape and is less affected by gravity gradient disturbance torques. This allows the presented 1U design with relatively low fin area to be sufficient for aerodynamic stability.

Table 5 describes the simulation parameters and results for the 1U CubeSat solution. Figure 19 shows the satellite response for the completely passive solution that uses magnetic hysteresis material for damping. We note that the attitude response shows improvement over the 3U CubeSat response plots; this is because of the smaller gravity gradient disturbance torques that the 1U satellite experiences in comparison.

Table 5. Design parameters and simulation results for 1U CubeSat with fins deployed at 50°.

1U CubeSat, 2.5 cm x 25 cm fins deployed at 50°		
Design Type	Passive Damping Solution	Active Damping Solution
Orbit	380 km circular, 51.6° inclination	
Mass, Inertia (Ixx, Iyy, Izz) Drag Area	1.33 kg, (0.00281, 0.003, 0.003) kg m^2 0.014788 m^2	
Angular Rate Damping	Hysteresis: HyMu80 0.9 cm^3 (0.3 cm^3 per axis)	B-dot control 0.04 Am^2 Torque Coils, K = 9000
Simulation Parameters	10 °/second initial rate	
Results		
Detumbling Time	5 hours	2 hours
Steady-state Tracking Accuracy	10-20°	Below 1°

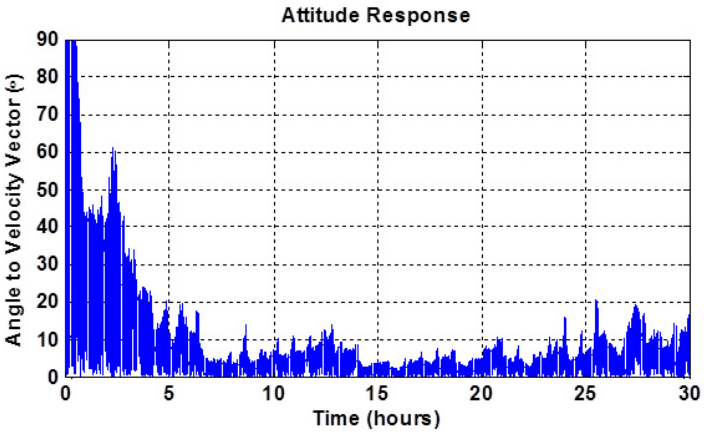

Figure 19. Simulated time response of aerostabilized 1U CubeSat with 2.5x25cm drag fins deployed at 50° and HyMu80 hysteresis damping.

For improved pointing accuracy, active rate damping can be employed. Using the same air core magnetic coils presented earlier driven by the B-dot control law, the attitude response of the active damping alternative is presented in Figure 20. Velocity vector tracking below 1° is achieved. The B-dot control gain was chosen to be K = 9000, resulting in an average total magnetic dipole of 0.00031 Am^2, with a maximum dipole of 0.001 Am^2 for any of the three coils in steady state.

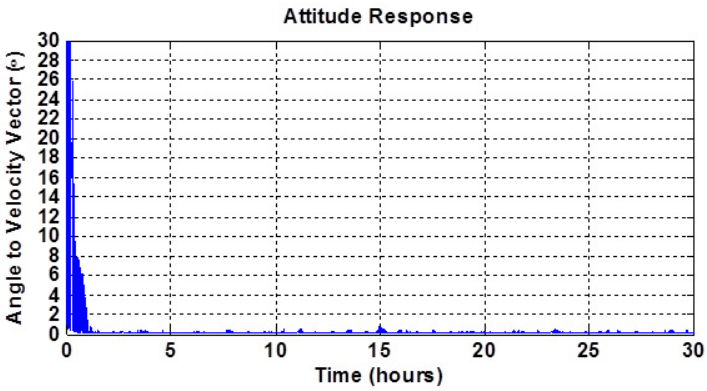

Figure 20. Simulated time response of aerostabilized 1U CubeSat with 2.5x25cm drag fins deployed at 50° and magnetic B-dot damping.

For the 380 km starting orbit, this design has an expected orbit lifetime of 3 – 14 months, depending on solar activity. The area-to-mass ratio of this design, which is key for orbit lifetime calculations, is highest of the previous designs and therefore has the shortest expected lifetime.

10. Discussion

10.1 Simulator Accuracy

Any simulation tool will have errors and inaccuracies associated with inaccuracies in satellite representation, numerical approximations, and modeling assumptions that are made. To gain confidence in the simulator, it was checked for accuracy against several satellites of known design parameters and on orbit results, including the NASA PAMS experiment, Delfi-C3, and QuakeSat (Rawashdeh and Lumpp, 2010). The verification applies to the simulation environment developed to generate the results presented in this paper.

The atmospheric density is assumed to be exponentially decreasing, but uniform at a certain altitude and constant at the average value for that altitude. In reality, the atmospheric density has a variance that increases with altitude, where at 500 km, for example, the atmospheric density can increase and decrease by an order of magnitude at the same altitude. In simulation, this can be compensated for by testing a certain design for various altitudes (in multiple simulations or in an elliptical orbit) to verify that a certain design would work. In addition, as presented in the simulation results, the aerodynamic design is not very sensitive as long as non-zero correcting torque is available, and is therefore not sensitive to small-scale variations in atmospheric density. The challenging part of the design was the magnetic hysteresis volume selection, which is independent of this assumption.

The density of the point cloud representation of the spacecraft geometry and the resolution of the torque profile look-up table were set to values that resulted in smooth curves for the torque profiles that are shown for all proposed designs. Emphasis was on the torque values at forward facing angles because the steady-state behavior was in question.

Simulink® is essentially a numerical differential equation solver. Numerical errors were observed when simulations were run with low relative tolerance settings for the solvers and long time steps. To mitigate interpreting numerical phenomena as actual expected behavior, for each case, multiple simulations are run using various differential equation solvers, tolerances, and time steps, until consensus is found. In addition, specific signal values, such the magnitude of torque values, hysteresis curve traces (Figure 5), and angular rates, are routinely checked for unreasonable values.

For the B-dot active magnetic damping solutions, perfect knowledge of magnetic field is assumed. It is expected that the errors associated with using a practical (non-ideal) magnetometer to read the magnetic field local to the spacecraft would propagate as noisy measurements of the time-derivative of the magnetic field ($\dot{B}$), and therefore adversely affect the actual control torques. Active damping is presented in this paper only to contrast passive damping as a proof of concept

for the order of magnitude aerodynamic and magnetic moment torques that are generated.

Some effects are not modeled in the simulations. Global horizontal winds are not modeled, and introduce an offset between the velocity vector and wind vector that is a function of orbit altitude and inclination. In addition, solar radiation pressure is not modeled. It was neglected for the ISS orbit in this work, where aerodynamic and gravity gradient torque dominated angular motion. Solar radiation torque should be considered at higher altitudes, for satellites with large cross-sectional areas, and when gravity gradient torque is negligible due to satellite symmetry.

10.2 Effect of Altitude on Passive Solutions

The discussion to this point has been specific to the ISS orbit altitude and inclination (380 km at 51.6°). Running the 3U CubeSat design with the same simulation parameters only increasing the orbit altitude showed reduced tracking accuracy. Specifically, errors to the velocity vector were up to 50° at 500 km, and 120° at 600 km, because of the diminishing atmospheric density. We note that solar radiation pressure becomes significant at these higher altitudes, further increasing the tracking error. When the orbit altitude was decreased below ISS altitudes, the same design also started showing increased errors of up to 30° at 350 km and 40° at 300 km. In this case, this is because of magnetic hysteresis material insufficiency, where lower altitudes experience larger aerodynamic torques, and would therefore need larger volumes of hysteresis material for damping.

It is therefore advised to design for the lowest altitude in the mission lifetime, where a design for lower altitudes is more likely to work well for higher altitudes than it is for lower altitudes.

10.3 Effect of Orbit Inclination on Magnetic Torques

Magnetic torques caused by the hysteresis material are key to the resulting effect of angular rate damping, therefore the Earth's magnetic field intensity and direction throughout the orbit in question merit consideration. The main factor is that magnetic torques suffer from incomplete control authority; as a property of magnetism, no torques vectors can be generated that are parallel to the magnetic field (Sidi, 1997). Running the 3U CubeSat design at ISS altitude while varying the orbit inclination showed improved performance for near equatorial orbits of inclinations under 10°. In those orbits, the magnetic field points north (i.e., it is perpendicular to the direction of travel, and has a relatively constant magnitude). No significant improvement was noticed for large inclinations near polar orbits. We note that polar orbits experience varying magnetic field directions throughout the orbit (nadir, anti-nadir, along travel, and opposite travel), and experience variations in magnitude, where the magnetic field is twice as strong at the poles than at the magnetic equator for the same altitude.

It is therefore advised to design the magnetic damping system for the lowest magnetic field expected for a certain orbit. In this case, stronger magnetic fields generate more damping, and as the orbit decays, the magnetic field intensity will increase as altitude decreases.

10.4 Aerodynamic and Hysteresis Design

At the 380 km orbit, the results show that the aerodynamic design did not have a great effect as long as the torque profile showed some measure of correcting torque for the forward-facing attitude. However, the design and stability were sensitive to the amount of hysteresis material. The optimal amount of hysteresis material required appears to scale with the inertia values of the satellite when comparing the 3U with the 1U designs.

10.5 Attitude Response

The attitude responses for the passive solutions show what appears to be sporadic behavior in steady-state. The attitude response is an aggregate of several orbital effects. Specifically, the magnitude and axis of gravity gradient torque are a function of attitude, as is the aerodynamic torque. Magnetic torques vary greatly as a function of attitude, especially because of the incomplete authority property of magnetic fields mentioned earlier, and this results in interesting dynamics.

In addition, as previously referenced in the magnetic coils section, changes of the magnetic field relative to the spacecraft body only approximate the actual rotations of the body. While hysteresis material and the B-dot control counter changes in the magnetic field, some changes are caused by the progression through orbit, and not by the spacecraft rotation. Furthermore, the magnetic field strength and direction changes occur on an orbital basis. Finally, the inclination of the Earth magnetic dipole relative to the orbital plane varies on a time scale of a day. The aggregate of all these effects produces response plots that appear to be unpredictable.

11. Conclusion

The Cosmos-147, Cosmos-320, and NASA PAMS spacecraft demonstrated aerodynamic stabilization with passive damping. This paper surveyed this previous work and extended the concept to the CubeSat form factor. An attitude propagator was developed, incorporating an orbit propagator, gravity gradient torques, aerodynamic torques, magnetic hysteresis torques, and the B-dot control law. The simulator was verified using flight results of several passively stabilized satellites and was used to design aerodynamically stable CubeSats.

The first set of designs is based on the Pumpkin Inc. Colony-1 Bus. The 3U CubeSats have side panels that deploy to trail the satellite, pushing the center of aerodynamic pressure behind the center of mass. Two deployment angles were proposed and analyzed for this shuttlecock configuration. The last design proposed an aerodynamically stable configuration for a 1U CubeSat. The 1U design incorporates drag fins based on flexible spring steel used in tape measure. The designs were shown to be feasible, using magnetic hysteresis for angular rate damping, with reasonable amounts of hysteresis material.

Under ideal circumstances where magnetic torquing does not adversely affect magnetometer readings, active damping is shown to significantly improve the tracking accuracy for all proposed designs with modestly strong air-core magnetic torque coils. The B-dot algorithm requires a magnetometer and 3-axis coils to provide improved damping. CubeSat solar boards with magnetometers and air-core coils are commercially available. An ideal magnetometer was assumed to provide a perfect measurement of the magnetic field vector for the damping algorithm, and Near-perfect tracking was observed. This paper concludes that the tracking accuracy in the active damping case is limited by the accuracy of the magnetic field measurement, which is a function of the quality of the magnetometer and magnetic field model.

The proposed designs can be assembled with off-the-shelf components, and provide a simple and low cost stable platform at the ISS orbit. Aerodynamic torques dominate attitude behavior at that altitude, driving the complexity and cost of other attitude control schemes. These designs are proposed as convenient platforms for short duration and repeatable experiments on upcoming ISS crew re-supply missions.

References

Abel, J. T. (2011): Development of a CubeSat instrument for microgravity particle damper performance analysis, M.S. Thesis, Cal. Poly. St. Univ., San Luis Obispo.

Armstrong, J., et al. (2009): Pointing control for low altitude triple CubeSat space darts, in *Proc. 23rd Annu. AIAA/USU Conf. Small Satellites,* Logan, UT.

Arnold, S., et al. (2012): QbX - The CubeSat experiment, in *Proc. 26th Annu. AIAA/USU Conf. Small Satellites,* Logan, UT.

Bjelde, B. (2011). SpaceX Keynote Address, Presented at: CubeSat Developer's Workshop, Cal. Poly. St. Univ. Available: http://mstl.atl.calpoly.edu/~bklofas/Presentations/DevelopersWorkshop2011/37_Bjelde_Keynote.pdf (accessed, January 2013).

California Polytechnic State University (CalPoly). (2012): CubeSat design specifications. Available: http://cubesat.org (accessed, January 2013).

Chandler, G. D., et al. (2007): Development of an off-the-shelf bus for small satellites, in *Proc. IEEE Aerospace Conference,* Big Sky, MT.

Cutler, J., et al. (2010): The Radio Aurora Explorer–A

bistatic radar mission to measure space weather phenomenon, in *Proc. 24th Annu. AIAA/USU Conf. Small Satellites,* Logan, UT.

Flatley, T. W. and Henretty, D. A. (1995): Technical Report N95- 27801: A Magnetic Hysteresis Model, NASA Goddard Space Flight Center, Greenbelt, MD: NASA Technical Reports Server.

GOM Space. (2012): NanoPower P100U-A. Available: http://gomspace.com/index.php?p=products-p100ua (accessed, August 2012).

K.E. Tsiolkovsky State Museum of the History of Cosmonautics. (2004-2012): Available: http://www.gmik.ru/index_en.html (accessed, August 2012).

Kumar, R. R., et al. (1995): Simulation and shuttle hitchhiker validation of passive satellite aerostabilization. *J. Spacecraft and Rockets*, 32 (5), pp. 806–811.

Kumar, R. R., et al. (1996): Parametric and classical resonance in passive satellite aerostabilization. *J. Spacecraft and Rockets,* 33(2), pp. 228–234.

Larson, W. J. and Wertz, J. R. (1999): *Space Mission Analysis and Design*, 3rd ed. Hawthorne, CA, Microcosm Press.

Levesque, J. (2003): Passive magnetic attitude stabilization using hysteresis materials, in Proc. *17th AIAA/USU Conf. Small Satellites,* Logan, UT.

NASA Goddard Space Flight Center. (1996): PAM's Update Page: Passive Aerodynamically Stabilized Magnetically Damped Satellite. Available: http://library01.gsfc.nasa.gov/host/hitchhiker/pams.html (accessed, January 2013).

NASA Johnson Space Center. (1996): Technical Report NSTS-37408: STS-77 Space Shuttle Mission Report. NASA Technical Reports Server.

NASA Orbital Debris Program Office. (2012): *Debris Assessment Software.* Available: http://orbitaldebris.jsc.nasa.gov (accessed, January 2013).

Pacini, L. and Skillman, D. (1995): A passive aerodynamically stabilized satellite for low Earth orbit, in . *Proc. AAS/AIAA Spaceflight Mechanics Mtg.*, Albuquerque, NM.

Psiaki, M. L. (2004): Nanosatellite attitude stabilization using passive aerodynamics and active magnetic torquing. *J. Guidance, Control, and Dynamics*, 27(3), pp. 347–355.

Pumpkin Incorporated. (2012): Available: http://www.cubesatkit.com (accessed, January 2013).

Rawashdeh, S. A. (2009): Passive attitude stabilization for small satellites, M.S. Thesis, Univ. Kentucky, Lexington.

Rawashdeh, S. A. and Lumpp, J. E. (2010): Nano-satellite passive attitude stabilization systems design by orbital environment modeling and simulation, in *Proc. AIAA Infotech@Aerospace Conf.*, Atlanta, GA.

Rawashdeh, S. A., et al. (2009): Aerodynamic attitude stabilization for a Ram-Facing CubeSat, in *Proc. AAS 32nd Annu. Guidance and Control Conf.*, Breckenridge, CO.

Sarychev, V. A.and Ovchinnikov, M. Y. (1994): Dynamics of a satellite with a passive aerodynamic attitude control system. *Cosmic Research,* 32(6), pp. 561-575.

Sarychev, V. A. et al. (1984): Optimal parameters of an aero-gyroscopic orientation system of satellites. *Cosmic Research,* 22(3), pp. 369-380.

Sarychev, V. A., et al. (2007): Equilibria of a satellite subjected to gravitational and aerodynamic torques with pressure center in a principal plane of inertia. *Celestial Mechanics and Dynamical Astronomy,* 100(4), pp. 301-318.

Schrello, D. M. (1961): Passive aerodynamic attitude stabilization of near Earth satellites. Declassified Research under United States Air Force Contract No. AF 33(616)-7100, North American Aviation Inc., Columbus, OH.

Sidi, M. J. (1997): *Spacecraft Dynamics and Control.* Cambridge, UK, Cambridge Univ. Press.

Silani, E.and Lovera, M. (2002): Magnetic spacecraft attitude control: a survey and some new results. *Control Engineering Practice,* 13(3), pp. 357-371.

U.S. Naval Research Laboratory. (2010): NRL launches nano-satellite experimental platforms. Available:http://www.nrl.navy.mil/media/news-releases/2010/nrl-launches-nanosatellite-experimental-platforms (accessed, September 2012).

University of Kentucky. (2013): Simulation tools: Smart Nanosatellite Attitude Propagator (SNAP). Space Systems Laboratory. Available: http://ssl.engineering.uky.edu/snap (accessed, January 2013).

Wade, M. (2012): DS-MO. *Encyclopedia Astronautica*. Available: http://www.astronautix.com/craft/dsmo.htm (accessed, January 2013).

Wall, J. K. (1959): The feasibility of aerodynamic attitude stabilization of a satellite vehicle. *American Rocket Society Preprints*, p. 787.

Waydo, S., et al. (2002): CubeSat design for LEO-based Earth science missions, in *Proc.IEEE Aerospace Conf.*, Big Sky, MT.

Wertz, J. R. (1978): *Spacecraft Attitude Determination and Control,* Dordrecht, Holland, D. Reidel Publishing Co.

Wie, B. (1998): *Space Vehicle Dynamics and Control.* Reston, VA, American Institute of Aeronautics and Astronautics Inc.